Dark Matter and Strong Electroweak Phase Transition in a Radiative Neutrino Mass Model

Amine Ahriche[1,*] and Salah Nasri[2,†]

[1]*Department of Physics, University of Jijel,*
PB 98 Ouled Aissa, DZ-18000 Jijel, Algeria.

[2]*Physics Department, UAE University,*
POB 17551, Al Ain, United Arab Emirates

(Dated: April 9, 2013)

Abstract

We consider an extension of the standard model (SM) with charged singlet scalars and right handed (RH) neutrinos all at the electroweak scale. In this model, the neutrino masses are generated at three loops, which provide an explanation for their smallness, and the lightest RH neutrino, N_1, is a dark matter candidate. We find that for three generations of RH neutrinos, the model can be consistent with the neutrino oscillation data, lepton flavor violating processes, N_1 can have a relic density in agreement with the recent Planck data, and the electroweak phase transition can be strongly first order. We also show that the charged scalars may enhance the branching ratio $h \to \gamma\gamma$, where as $h \to \gamma Z$ get can get few percent suppression. We also discuss the phenomenological implications of the RH neutrinos at the collider.

PACS numbers: 95.35.+d; 98.80.-k; 12.15.-y; 11.30.Qc.

Keywords: Charged scalars, WIMP's, Higgs diphoton decay, electroweak phase transition.

*Electronic address: ahriche@univ-jijel.dz

†Electronic address: snasri@uaeu.ac.ae

I. INTRODUCTION

There are three concrete evidences for Physics beyond the standard model (SM): (i) non zero neutrino masses, (ii) the existence of dark matter (DM), and (iii) the observation of matter anti matter asymmetry of the universe. However, most of the SM extensions make no attempt to address these three puzzles within the same framework. For instance, in the minimal supersymmetric standard model (MSSM), the lightest supersymmetric particle (LSP) is a candidate for DM and, in principle, has the necessary ingredients to generate the baryon asymmetry of the universe (BAU), but it does not provide an explanation for why neutrino masses are tiny. Moreover, direct searches for supersymmetric particles have yielded null results so far. Another popular extension of the SM, is introducing very heavy right -handed (RH) neutrinos ($m_N \geq 10^8$ GeV, where small neutrino masses are generated via the see-saw mechanism [1], and the BAU is produced via leptogenesis [2]. Unfortunately, such heavy particles decouple from the effective low energy theory and can not be tested at collider experiments. In addition, for m_N heavier than 10^7 GeV, the Dirac neutrino mass term induces large corrections to the Higgs mass, which can destabilize the electroweak vacuum [3].

Another possible way to understand the smallness of neutrino masses is to generate them radiatively. The famous example is the so-called Zee model [4], where one augments the scalar sector of the SM with a Higgs doublet, and a charged field which transforms as a singlet under $SU(2)_L$, which leads to non zero neutrino mass at one loop level. However, the solar mixing angle comes out to be close to maximal, which is excluded by the solar neutrino oscillation data [5]. This problem is circonvented in models where neutrinos are induced at two loops [6] or three loops [7–9]. One of the advantages of this class of models is that all the mass scales are in the TeV or sub-TeV range, which makes it possible for them to be tested at future colliders.

In Ref. [7], the SM was extended with two electrically charged $SU(2)_L$ singlet scalars and one RH neutrino field, N, where a Z_2 symmetry was imposed to forbid the Dirac neutrino mass terms at tree level [7]. Once the electroweak symmetry is broken, neutrino masses are generated at three loops, naturally explaining why their masses are so tiny compared to the charged leptons as due to the high loop suppression. A consequence of the Z_2 symmetry and the field content of the model, N is Z_2-odd, and thus guaranteed to be stable, which

make it a good DM candidate. In Ref. [10], the authors considered extending the fermion sector of the SM with two RH neutrinos, in order to for it to be consistent with the neutrino oscillation data, and they studied also its phenomenological implications.

Here, we calculate the three loop neutrino masses exactly, as compared to the approximate expression derived in [7]. We show that in order to satisfy the recent experimental bound on the lepton flavor violating (LFV) process such as $\mu \to e\gamma$ [11]; and the anomalous magnetic moment of the muon [12], one must have three generations of RH neutrinos. Taking into account the neutrino oscillation data and the LFV constraints, we show that the lightest RH neutrino can account for the DM abundance with masses lighter than 225 GeV. The presence of the charged scalars in this model will affect the Higgs decay process $h \to \gamma\gamma$ and can lead to an enhancement with respect to the SM, where as $h \to \gamma Z$ is slightly reduced. In this model, we find that a strongly electroweak phase transition can be achieved with a Higgs mass of $\simeq 125$ GeV as measured at the LHC [13, 14].

This paper is organized as follows. In the next section we present the model, and discuss the constraints from the LFV processes. In section III, we study the relic density of the lightest RH neutrino, and discuss the coannihilation effect due to the next lightest RH neutrino. Section IV is devoted to the study of the electroweak phase transition. In section V, we discuss the phenomenological implications of the RH neutrinos at electron-positron colliders. Finally we conclude in section VI. The formula of the three loop factor that enters in the expression of the neutrino masses is derived in Appendix A. In Appendix B, we give the shift in masses the gauge bosons and the scalars at finite temperature.

II. NEUTRINO DATA AND FLAVOR VIOLATION CONSTRAINTS

In this section, we define the filed content of the model, give the exact expression of the neutrino masses, and discuss the constraints from LFV processes.

A. The Model

Here we consider extending the SM with three right-handed neutrinos, N_i, and two electrically charged scalars, $S_1^{\pm}$ and $S_2^{\pm}$, that are singlet under $SU(2)_L$ gauge group. In addition, we impose a discrete Z_2 symmetry on the model, under which $\{S_2, N_i\} \to \{-S_2, -N_i\}$, and

all other fields are even. The Lagrangian reads

$$\begin{aligned}\mathcal{L} = \mathcal{L}_{SM} + \{ & f_{\alpha\beta} L_\alpha^T C i\tau_2 L_\beta S_1^+ + g_{i\alpha} N_i S_2^+ \ell_{\alpha R} \\ & + \tfrac{1}{2} M_{N_i} N_i^C C N_i + h.c\} - V(\Phi, S_1, S_2),\end{aligned} \tag{2.1}$$

where, L_α is the left-handed lepton doublet, C is the charge conjugation matrix, $f_{\alpha\beta}$ are Yukawa couplings which are antisymmetric in the generation indices α and β, and $V(\Phi, S_1, S_2)$ is the tree-level scalar potential which is given by

$$\begin{aligned}V(\Phi, S_{1,2}) = {} & \lambda \left(|\Phi|^2\right)^2 - \mu^2 |\Phi|^2 + m_1^2 S_1^* S_1 + m_2^2 S_2^* S_2 + \lambda_1 S_1^* S_1 |\Phi|^2 + \lambda_2 S_2^* S_2 |\Phi|^2 \\ & + \frac{\eta_1}{2} \left(S_1^* S_1\right)^2 + \frac{\eta_2}{2} \left(S_2^* S_2\right)^2 + \eta_{12} S_1^* S_1 S_2^* S_2 + \{\lambda_s S_1 S_1 S_2^* S_2^* + h.c\}\,.\end{aligned} \tag{2.2}$$

Here Φ denotes the SM Higgs doublet. It is worth mentioning that, the charge breaking minima are not possible due to the positive-definite values of λ_s and η_{12}; in addition to the conditions on the charged scalar masses $m_{S_{1,2}}^2 = m_{1,2}^2 + \lambda_{1,2} v^2/2 > 0$.

There are two immediate implications of the Z_2 symmetry imposed on the Lagrangian:

- First, if N_1 is the lightest particle among N_2, N_3, S_1 and S_2, then it would be stable, and hence it would be a candidate for dark matter. Moreover, N_i will be pair produced and subsequently decay into N_1 (or to N_2 and then to N_1) and a pair (or two pairs) of charged leptons. We will discuss its phenomenology in section VI.

- The second implication, is that the Dirac neutrino mass term is forbidden at all levels of the perturbation theory, and Majorana neutrinos masses are generated radiatively at three-loops, as shown in Fig. 1.

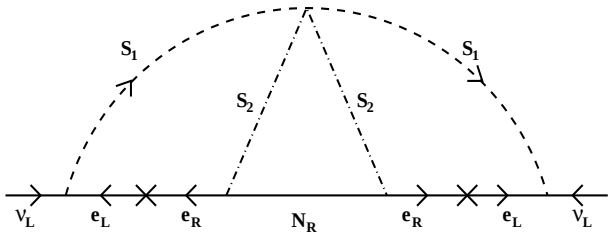

FIG. 1: *The three-loop diagram that generates the neutrino mass.*

B. Neutrino mass

The neutrino mass matrix elements arising from the three-loop diagram in Fig. 1, are given by

$$(M_\nu)_{\alpha\beta} = \frac{\lambda_s m_{\ell_i} m_{\ell_k}}{(4\pi^2)^3 m_{S_2}} f_{\alpha i} f_{\beta k} g_{ij} g_{kj} F\left(m_{N_j}^2/m_{S_2}^2, m_{S_1}^2/m_{S_2}^2\right), \tag{2.3}$$

where $\rho, \kappa (= e, \mu, \tau)$ are the charged leptons flavor indices, $i = 1, 2, 3$ denotes the three right-handed neutrinos, and the function F is a loop integral given in (A8), which was approximated to one in the original work [7]. Note that, unlike the conventional seesaw mechanism, the radiatively generated neutrino masses are directly proportional to the charged leptons and RH neutrino masses as shown in (2.3) and (A8).

In general, the elements of the neutrino mass matrix can be written as

$$(M_\nu)_{\alpha\beta} = [U \cdot diag(m_1, m_2, m_3) \cdot U^T]_{\alpha\beta}, \tag{2.4}$$

where U is the Pontecorvo-Maki-Nakawaga-Sakata (PMNS) mixing matrix [15], which is parameterized in general by

$$U = \begin{pmatrix} c_{12}c_{13} & c_{13}s_{12} & s_{13}e^{-i\delta_D} \\ -c_{23}s_{12} - c_{12}s_{13}s_{23}e^{i\delta_D} & c_{12}c_{23} - s_{12}s_{13}s_{23}e^{i\delta_D} & c_{13}s_{23} \\ s_{12}s_{23} - c_{12}c_{23}s_{13}e^{i\delta_D} & -c_{12}s_{23} - c_{23}s_{12}s_{13}e^{i\delta_D} & c_{13}c_{23} \end{pmatrix} \begin{pmatrix} 1 & 0 & 0 \\ 0 & e^{i\alpha/2} & 0 \\ 0 & 0 & e^{i\beta/2} \end{pmatrix}, \tag{2.5}$$

with $s_{ij} \equiv \sin(\theta_{ij})$ and $c_{ij} \equiv \cos(\theta_{ij})$, δ_D is the Dirac phase; and α and β are the Majorana phases. Using the experimental allowed values for $s_{12}^2 = 0.320^{+0.016}_{-0.017}$, $s_{23}^2 = 0.43^{+0.03}_{-0.03}$, $s_{13}^2 = 0.025^{+0.003}_{-0.003}$, $|\Delta m_{31}^2| = 2.55^{+0.06}_{-0.09} \times 10^{-3}$ eV^2 and $\Delta m_{21}^2 = 7.62^{+0.19}_{-0.19} \times 10^{-5}$eV^2 [16], we can find the parameter space of the model that is consistent with the neutrino oscillation data.

C. Experimental constraints

Besides neutrino masses and mixing, the Lagrangian (2.1) induces flavor violating processes such as $\ell_\alpha \to \gamma \ell_\beta$ if $m_{\ell_\alpha} > m_{\ell_\beta}$, generated at one loop via the exchange of both extra charged scalars $S_{1,2}^\pm$. The branching ratio of such process can be computed following [17] as

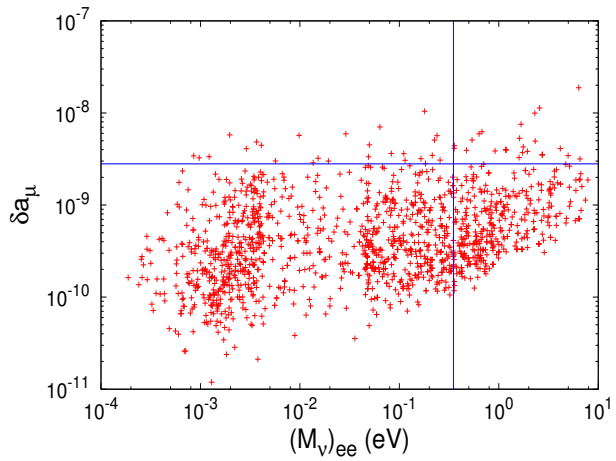

FIG. 2: *The muon anomalous magnetic moment versus the $\beta\beta_{0\nu}$ decay effective Majorana $(M_\nu)_{ee}$. The blue lines represent their experimental upper bounds.*

[1]

$$B(\ell_\alpha \to \gamma \ell_\beta) = \frac{\Gamma(\ell_\alpha \to \gamma \ell_\beta)}{\Gamma(\ell_\alpha \to \ell_\beta \nu_\alpha \bar{\nu}_\beta)}$$
$$= \frac{\alpha_{em} v^4}{384\pi} \left\{ \frac{\left| f_{\kappa\alpha} f^*_{\kappa\beta} \right|^2}{m^4_{S_1}} + \frac{36}{m^4_{S_2}} \left| \sum_i g_{i\alpha} g^*_{i\beta} F_2 \left(\frac{m^2_{N_i}}{m^2_{S_2}} \right) \right|^2 \right\}, \tag{2.6}$$

with $\kappa \neq \alpha, \beta$, α_{em} is the fine structure constant and $F_2(x) = (1 - 6x + 3x^2 + 2x^3 - 6x^2 \ln x)/6(1-x)^4$. For the case of $\ell_\alpha = \ell_\beta = \mu$, this leads to a new contribution to the muon anomalous magnetic moment δa_μ, that is given by

$$\delta a_\mu = \frac{m^2_\mu}{16\pi^2} \left\{ \frac{|f_{\mu e}|^2 + |f_{\mu\tau}|^2}{6 m^2_{S_1}} + \frac{1}{m^2_{S_2}} \sum_i |g_{i\mu}|^2 F_2 \left(\frac{m^2_{N_i}}{m^2_{S_2}} \right) \right\}. \tag{2.7}$$

In Fig. 2, we show a scattered plot of the muon anomalous magnetic moment versus the $\beta\beta_{0\nu}$ decay effective Majorana mass $(M_\nu)_{ee}$. In our scan of the parameter space of the model, we took $m_{S_{1,2}} \geq 100$ GeV**;** and demanded that (2.3) to be consistent with the neutrino oscillation data. From Fig. 2, one can see that most of the values of $(M_\nu)_{ee}$ that are consistent with the bound on δa_μ are lying in the range 10^{-3} eV to $\sim$eV. The current bound on $(M_\nu)_{ee}$ is approximately 0.35 eV [19] and it is expected that within few years a number of next generation $\beta\beta_{0\nu}$ experiments will be sensitive to $(M_\nu)_{ee} \sim 10^{-2}$ eV [20].

[1] One has to mention that this results is different from Eq. (38) in [18], where the authors took the summation over the square of the $g_{i\alpha}$ terms instead of the square of the their summation. The latter allows the parameter space of couplings to be enlarged.

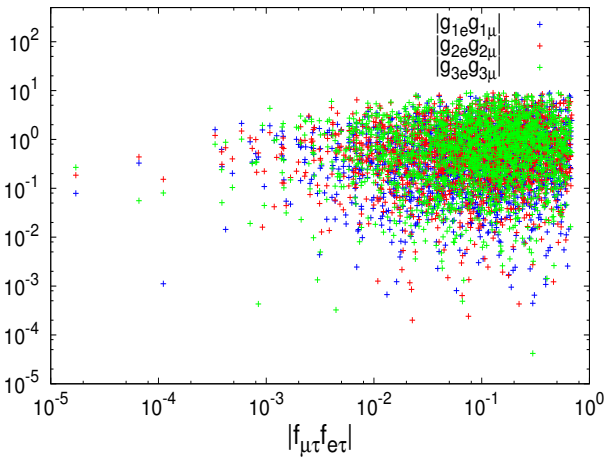

FIG. 3: *Different parameters combinations (as absolute values) that are relevant to the LFV constrain on $B(\mu \to e\gamma)$, are shown where (2.3) and (2.4) are matched.*

Fig. 3 gives an idea about the magnitude of the couplings that satisfy the constraints from LFV processes and the muon anomalous magnetic moment, and which also are consistent with the neutrino oscillation data. It is worth noting that when considering just two generations of RH neutrinos (i.e, $g_{3\alpha} = 0$), we find that the bound on the experimental bound $B\left(\mu \to e\gamma\right) < 5.7 \times 10^{-13}$ is violated [11][2]. Therefore, having three RH neutrinos is necessary for it to be in agreement with the data from the bounds from LFV processes.

III. DARK MATTER, COANNIHILATION EFFECT & INDIRECT DETECTION

A. Relic density

As we noted earlier, the lightest RH neutrino N_1 is stable, and could be the DM candidate. In the case of hierarchical RH neutrino mass spectrum, we can safely neglect the effect of N_2 and N_3 on N_1 density. The N_1 number density get depleted through the annihilation process $N_1 N_1 \to \ell_\alpha \ell_\beta$ via the t-channel exchange of $S_2^\pm$. For two incoming dark matter particles with momenta p_1 and p_2, and final states charged leptons with momenta k_1 and k_2, the amplitude for this process is

$$\mathcal{M}_{\alpha\beta} = g_{1\alpha} g_{1\beta}^* \left[\frac{\bar{u}(k_1) P_L u(p_1).\bar{v}(p_2) P_R v(k_2)}{t - m_{S_2}^2} - \frac{\bar{u}(k_1) P_L u(p_2).\bar{v}(p_1) P_R v(k_2)}{u - m_{S_2}^2} \right], \tag{3.1}$$

[2] Although, we have considered the bound on $B(\tau \to \mu\gamma) < 4.5 \times 10^{-8}$ [12], in our numerical scan, it does constrain severely the parameter space of the model.

where $t = (p_1 - k_1)^2$ and $u = (p_1 - k_2)^2$ are the Mandelstam variables corresponding the t and u channels, respectively. After squaring, summing and averaging over the spin states, we find that in the non-relativistic limit, the total annihilation cross section is given by

$$\sigma_{N_1 N_1} \upsilon_r \simeq \sum_{\alpha,\beta} |g_{1\alpha} g_{1\beta}^*|^2 \frac{m_{N_1}^2 \left(m_{S_2}^4 + m_{N_1}^4\right)}{48\pi \left(m_{S_2}^2 + m_{N_1}^2\right)^4} \upsilon_r^2, \tag{3.2}$$

with υ_r is the relative velocity between the annihilation N_1's. As the temperature of the universe drops below the freeze-out temperature $T_f \sim m_{N_1}/25$, the annihilation rate becomes smaller than the expansion rate (the Hubble parameter) of the universe, and the N_1's start to decouple from the thermal bath. The relic density after the decoupling can be obtained by solving the Boltzmann equation, and it is approximately given by

$$\begin{aligned} \Omega_{N_1} h^2 &\simeq \frac{2x_f \times 1.1 \times 10^9 \text{GeV}^{-1}}{\sqrt{g_*} M_{pl} \langle \sigma_{N_1 N_1} \upsilon_r \rangle} \\ &\simeq \frac{1.28 \times 10^{-2}}{\sum_{\alpha,\beta} |g_{1\alpha} g_{1\beta}^*|^2} \left(\frac{m_{N_1}}{135 \text{ GeV}}\right)^2 \frac{\left(1 + m_{S_2}^2/m_{N_1}^2\right)^4}{1 + m_{S_2}^4/m_{N_1}^4}, \end{aligned} \tag{3.3}$$

where $< \upsilon_r^2 > \simeq 6/x_f \simeq 6/25$ is the thermal average of the relative velocity squared of a pair of two N_1 particles, M_{pl} is planck mass; and $g_*(T_f)$ is the total number of effective massless degrees of freedom at T_f.

In Fig. 4, we plot the allowed mass range (m_{N_1}, m_{S_i}) plane that give the observed dark matter relic density [21]. As seen in the figure, the neutrino experimental data combined with the relic density seems to prefer $m_{S_1} > m_{S_2}$ for large space of parameters. However, the masses of both the DM and the charged scalar $S_2^\pm$ can not exceed $m_{N_1} < 225$ GeV and $m_{S_2} < 245$ GeV, respectively.

B. Coannihilation effect

In computing the relic density in (3.3), we have assumed that there is a hierarchy between the three right-handed neutrino masses. However, if we consider the possibility for N_2 and/or N_3 being close in mass to N_1, i.e $\Delta_i = (m_{N_i} - m_{N_1})/m_{N_1} << 1$, then coannihilation processes like $N_1 N_{2,3} \to \ell_\alpha \ell_\beta$ might have important effects on the evolution of the N_1-number density. The process $N_1 S_2^\pm \to \ell_\alpha^\pm \gamma$ is suppressed by the large mass difference between $S_2^\pm$ and N_1 and the smallness of the electromagnetic coupling compared to $\mathcal{O}(g^2)$, and therefore its contribution to the coannihilation is negligible.

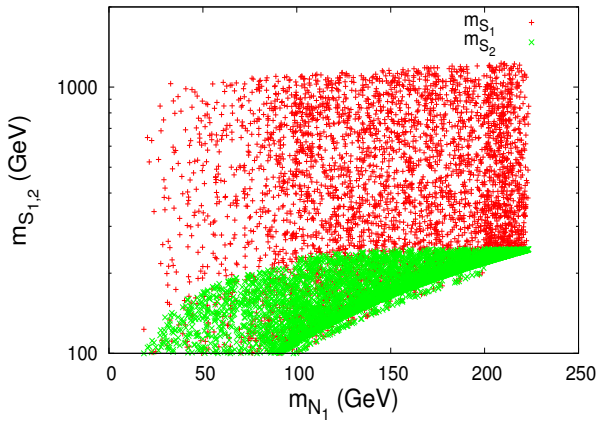

FIG. 4: *The charged scalar masses m_{S_1} (red) and m_{S_2} (green) versus the lightest RH neutrino mass, where the consistency with the neutrino data, LFV constraints and the DM relic density have been imposed.*

Following [22], the coannihilation effect could be included by re-evaluating the relic density (3.3) using the effective annihilation cross section and multiplicity

$$\begin{aligned} \sigma_{eff}(x) &= \sum_{i,k}^{3} \frac{2^2}{g_{eff}^2} \left(1+\Delta_i\right)^{3/2} \left(1+\Delta_k\right)^{3/2} e^{-x(\Delta_i+\Delta_k)} \sigma\left(N_i N_k \to \ell_\alpha^- \ell_\beta^+\right), \\ g_{eff}(x) &= \sum_{i}^{3} 2 \left(1+\Delta_i\right)^{3/2} e^{-x\Delta_i}, \end{aligned} \tag{3.4}$$

For freeze-out temperature much smaller than m_{N_1}, the effective cross section can be written as $\sigma_{eff}(x)\upsilon_r = a_{eff}(x) + b_{eff}(x)\upsilon_r^2 + \mathcal{O}\left(\upsilon_r^4\right)$, where

$$\begin{aligned} a_{eff}(z) &= \sum_{ik} a_{ik} \frac{2^2}{g_{eff}^2(z)} \left(1+\Delta_i\right)^{3/2} \left(1+\Delta_k\right)^{3/2} e^{-z(\Delta_i+\Delta_k)}, \\ b_{eff}(z) &= \sum_{ik} b_{ik} \frac{2^2}{g_{eff}^2(z)} \left(1+\Delta_i\right)^{3/2} \left(1+\Delta_k\right)^{3/2} e^{-z(\Delta_i+\Delta_k)}. \end{aligned} \tag{3.5}$$

Here the factors a_{ik} and b_{ik} correspond to the two first terms in the velocity expansion of $\sigma\left(N_i N_k \to \ell_\alpha^+ \ell_\beta^-\right)\upsilon_r$ (i.e, the s and p wave terms, respectively), given by

$$\begin{aligned} a_{ik} &= \frac{1}{32\pi} \sum_{\alpha,\beta} \left| g_{i\alpha} g_{k\beta}^* - g_{i\beta}^* g_{k\alpha} \right|^2 \frac{m_{N_i} m_{N_k}}{\left(m_{N_i}^2 + m_{S_2}^2\right)\left(m_{N_k}^2 + m_{S_2}^2\right)}, \\ b_{ik} &= \frac{m_{N_i} m_{N_k}}{48\pi \left(m_{N_i}^2 + m_{S_2}^2\right)^2 \left(m_{N_k}^2 + m_{S_2}^2\right)^2} \left\{ \sum_{\alpha,\beta} \left| g_{i\alpha} g_{k\beta}^* \right|^2 \left(m_{N_i}^2 m_{N_k}^2 + m_{S_2}^4 \right) \right. \\ &\left. + \frac{1}{2} \sum_{\alpha,\beta} \left| g_{i\alpha} g_{k\beta}^* - g_{i\beta}^* g_{k\alpha} \right|^2 \left(m_{S_2}^4 - 3 m_{N_i} m_{N_k} m_{S_2}^2 - m_{N_i}^2 m_{N_k}^2 \right) \right\}. \end{aligned} \tag{3.6}$$

Thus, the coannihilation effect on the relic density could be accounted for by just multiplying the couplings term $\sum_{\alpha,\beta}|g_{1\alpha}g_{1\beta}^*|^2$ in (3.3) by the factor

$$\kappa = \left(\frac{x_f'}{x_f}\right)^{-1}\left(\frac{g_*(x_f')}{g_*(x_f)}\right)^{1/2}\frac{I_a(x_f')+I_b(x_f')\upsilon_r'^2}{b_{11}\upsilon_r^2}. \tag{3.7}$$

Here $x_f' = m_{N_1}/T_f'$ is the freeze-out temperature defined using $\sigma_{eff}(x)\upsilon_r$ instead of $\sigma_{N_1N_1}\upsilon_r$, and the integral functions $I_a(x)$ and $I_b(x)$ are given by

$$I_a(x) = x\int_x^\infty a_{eff}(z)z^{-2}dz,\ I_b(x) = 2x^2\int_x^\infty b_{eff}(z)z^{-3}dz, \tag{3.8}$$

which, in general, causes a shift in the freeze-out temperature. In our case, we find that x_f gets lowered by less then 3% for $\Delta_{2,3}$ for $5\% < \Delta_{2,3} < 25\%$, and therefore, within this range, the effect of coannihilation on the freeze-out temperature and $g_*(x_f)$ can be ignored and one approximate the factor κ by the ratio $(I_a(x_f)+I_b(x_f)\upsilon_r^2)/b_{11}\upsilon_r^2$. However for $\Delta_{2,3} << 5\%$, x_f can be shifted by more then a factor of two, which results in a freeze-out temperature of about 50 MeV. Hence, for N_1 to have the observed cosmological relic density, it must must be that

$$\kappa\sum_{\alpha,\beta}|g_{1\alpha}g_{1\beta}|^2 = (114.04 \pm 3.56)\times 10^{-3}\times\left(\tfrac{m_{N_1}}{135\ \text{GeV}}\right)^2\frac{\left(1+m_{S_2}^2/m_{N_1}^2\right)^4}{1+m_{S_2}^4/m_{N_1}^4}, \tag{3.9}$$

In Fig. 5, we plot the ratio $\Omega_{N_1}'h^2/\Omega_{N_1}h^2$ versus m_{N_1}, where $\Omega_{N_1}h^2(\Omega_{N_1}'h^2)$ is the relic density estimated without (with) coannihilation effect. We see that for $\Delta_1 \lesssim 0.05$, the coannihilation becomes significant and leads to an increase in the relic density by more then 50%, whereas for $\Delta_1 \lesssim 0.01$, this increase is almost factor of three.

C. Indirect Detection constrains

Before closing this section, we would like to comment on the detection of the dark matter in our model.

- The direct detection: Since the interactions of N_1 involve only leptons, the N_1-nucleon scattering is absent at the tree level. Moreover, it can not scatter via electromagnetic interaction since the dipole moment for Majorana particles vanish identically. However, if N_1 and N_2 (or N_3) are quasi-degenerate, then a transition magnetic dipole moment can be generated radiatively, and in that case an inelastic scattering $N_1+p \to N_2+p$ is possible, provided that $\Delta_1 \leq 10^{-6}\left(\frac{10\ \text{GeV}}{m_{N_1}}\right)$. It is quite unlikely

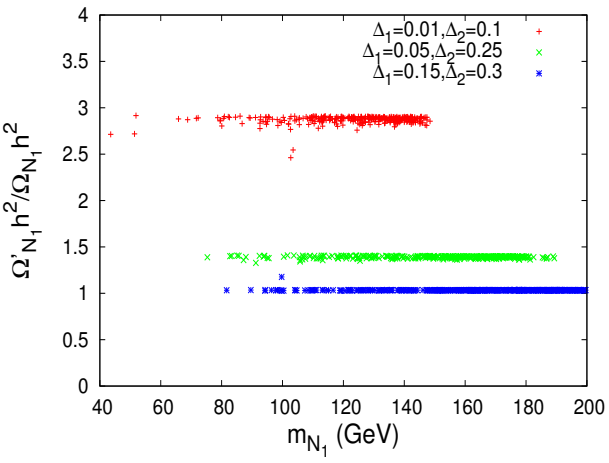

FIG. 5: *The ratio $\Omega'_{N_1}h^2/\Omega_{N_1}h^2$ versus the lightest RHN mass m_{N_1}, where $\Omega_{N_1}h^2$ ($\Omega'_{N_1}h^2$) is the N_1 relic density without (with) the coannihilation effect.*

that such a tiny degeneracy will be stable under the radiative correction to m_{N_1} and m_{N_2} generated via one loop diagrams by the exchange of S_2 and charged leptons.

- The indirect detection: The N_1 annihilation rate into leptons has a helicity suppressed s-wave term (i.e. $\propto m_l^2/m_{N_1}^2$) and a p-wave contribution. For $m_{N_1} \geq 100$ GeV, both terms can be of the same order for $g_{1\tau} \sim 1$. Unfortunately, with the dark matter velocity in the galactic halo of the order 10^{-3}, the cross section is too small to have a chance for the annihilation products of N_1 to be detected. This helicity suppression of the s-wave will be lifted if the final state have in addition a spin one particle. This is the case for the internal bremsstrahlung (IB) processes, where a photon is emitted from the final state charged leptons (FSR) or from charged mediator in the t-channel propagator (VIB) [3]. The later exhibits an enhancement for large photon energies if the dark matter and the particle in the propagator, whereas the FSR is dominated by the photons that are approximately collinear with either ℓ_α or ℓ_β. The annihilation process $N_1N_1 \to \ell_\alpha\ell_\beta\gamma$ not only could have a larger cross section then $N_1N_1 \to \ell_\alpha\ell_\beta$ but also leads to a gamma ray signal with a sharp spectral features that is potentially observable at future gamma-ray telescopes. Very recently [23], It has been shown that in this model, a DM with the mass m_{N_1} ∼135 GeV could lead to

[3] Although the soft and collinear FSR is logarithmically enhanced, it is helicity suppressed, and thus typically smaller then VIB . However, they have to be both included to obtain a gauge invariant result.

the following three effects: (1) a wide internal bremsstrahlung bump with maximum of $90\% m_{N_1}$ ∼120 GeV, (2) a $\gamma\gamma$ line around $E_\gamma = m_{N_1}$ ∼135 GeV, and (3) a $Z\gamma$ line at $E_\gamma = m_{N_1}(1 - m_Z^2/(4m_{N_1}^2))$ ∼119.6 GeV. These features together provide a good fit to the gamma rays excess observed in the Fermi-LAT data [23].

IV. THE HIGGS DECAY CHANNELS $h \to \gamma\gamma$ AND $h \to \gamma Z$

Recently, ATLAS [24] and CMS [25] collaborations have announced the observation of a scalar particle with mass $\simeq 125$ GeV at about 5 σ confidence level. The question is whether or not this is really the SM Higgs or some Higgs-like state with different properties. Indeed, the fit of the data by the ATLAS collaboration seems to show an excess in $h \to \gamma\gamma$ events by more than 50% with respect to the SM, while the updated CMS analysis is consistent with the SM. Defining $R_{\gamma\gamma}$ to be the decay width of $h \to \gamma\gamma$ scaled by its expected SM value, we find that

$$R_{\gamma\gamma} = \left| 1 + \frac{v^2}{2} \frac{\frac{\lambda_1}{m_{S_1}^2} A_0\left(\tau_{S_1}\right) + \frac{\lambda_2}{m_{S_2}^2} A_0\left(\tau_{S_2}\right)}{A_1\left(\tau_W\right) + N_c Q_t^2 A_{1/2}\left(\tau_t\right)} \right|^2 , \tag{4.1}$$

where $\tau_X = m_h^2/4m_X^2$, with m_X is the mass of the charged particle X running in the loop, $N_c = 3$ is the color number, and Q_t is the electric charge of the top quark in unit of $|e|$. The loop amplitudes A_i for spin 0, spin 1/2 and spin 1 particle contribution are given by [26]

$$\begin{aligned} A_0\left(x\right) &= -x^{-2}\left[x - f\left(x\right)\right], \\ A_{1/2}\left(x\right) &= 2x^{-2}\left[x + \left(x-1\right) f\left(x\right)\right], \\ A_1\left(x\right) &= -x^{-2}\left[2x^2 + 3x + 3\left(2x-1\right) f\left(x\right)\right], \end{aligned} \tag{4.2}$$

with

$$f\left(x\right) = \begin{cases} \arcsin^2\left(\sqrt{x}\right) & x \le 1 \\ -\frac{1}{4}\left[\log\frac{1+\sqrt{1-x^{-1}}}{1-\sqrt{1-x^{-1}}} - i\pi\right]^2 & x > 1. \end{cases} \tag{4.3}$$

The effect on the $B(h \to \gamma\gamma)$ charged scalar singlets will depend on how light are $S_{1,2}^{\pm}$, the sign and the strength of their couplings to the SM Higgs doublet. For instance, an enhancement can be achieved by taking λ_1 and/or λ_2 to be negative.

Another Higgs decay channel that could be modified due to these extra charged fields, is

the process $h \to \gamma Z$, where similarly the effect is parameterized by

$$R_{\gamma Z} = \left| 1 + s_w^2 \frac{v^2}{2} \frac{\frac{\lambda_1}{m_{S_1}^2} A_0\left(\tau_{S_1}, \zeta_{S_1}\right) + \frac{\lambda_2}{m_{S_2}^2} A_0\left(\tau_{S_2}, \zeta_{S_2}\right)}{c_w A_1\left(\tau_W, \zeta_W\right) + \frac{2(1-8s_w^2/3)}{c_w} A_{1/2}\left(\tau_t, \zeta_t\right)} \right|^2 , \tag{4.4}$$

where $\zeta_X = m_Z^2/4m_X^2$, and the A's functions here are given by [26]

$$\begin{aligned} A_0\left(x,y\right) &= I_1\left(x,y\right), \\ A_{1/2}\left(x,y\right) &= I_1\left(x,y\right) - I_2\left(x,y\right), \\ A_1\left(x,y\right) &= \left[(1+2x)\tan^2\theta_w - (5+2x)\right] I_1\left(x,y\right) + 4\left(3 - \tan^2\theta_w\right) I_2\left(x,y\right), \end{aligned} \tag{4.5}$$

with

$$\begin{aligned} I_1\left(x,y\right) &= -\tfrac{1}{2(x-y)} + \tfrac{f(x)-f(y)}{2(x-y)^2} + \tfrac{y[g(x)-g(y)]}{(x-y)^2}, \\ I_2\left(x,y\right) &= \tfrac{f(x)-f(y)}{2(x-y)}, \end{aligned} \tag{4.6}$$

and

$$g\left(x\right) = \begin{cases} \sqrt{x^{-1}-1}\arcsin\left(\sqrt{x}\right) & x \le 1 \\ \frac{\sqrt{1-x^{-1}}}{2}\left[\log\frac{1+\sqrt{1-x^{-1}}}{1-\sqrt{1-x^{-1}}} - i\pi\right] & x > 1. \end{cases} \tag{4.7}$$

In Fig. 6, we present $R_{\gamma\gamma}$ versus $R_{\gamma Z}$ for randomly chosen sets of parameters where the charged scalars are taken to be heavier than 100 GeV, the Higgs mass within the range $124 < m_h < 126$ GeV, and the condition of a strongly first order phase transition is implemented (see next section). In our numerical scan, we take the model parameters relevant for the Higgs decay to be in the range

$$\lambda < 2, \;\; |\lambda_{1,2}| < 3, \;\; m_{1,2}^2 < 2 \text{ TeV}^2, \tag{4.8}$$

where the Higgs mass is calculated at one-loop level. An enhancement of $B(h \to \gamma\gamma)$ can be obtained for a large range of parameter space, whereas $B(h \to \gamma Z)$ is slightly reduced with respect to the SM. It is interesting to note that if one consider the combined ATLAS and CMS di-photon excess, then $R_{\gamma Z}$ is predicted to be smaller than the expected SM value by approximately 5%.

V. A STRONG FIRST ORDER ELECTROWEAK PHASE TRANSITION

It is well known that the SM has all the qualitative ingredients for electroweak baryogenesis, but the amount of matter-antimatter asymmetry generated is too small. One of

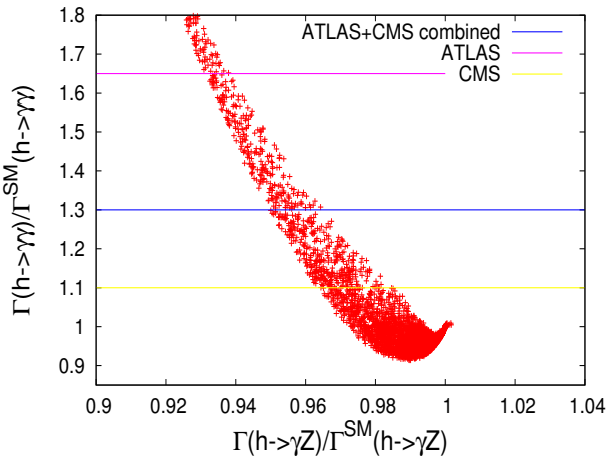

FIG. 6: *The modified Higgs decay rates $B(h \to \gamma\gamma)$ vs $B(h \to \gamma Z)$, scaled by their SM values, due to the extra charged scalars, for randomly chosen sets of parameters. The magenta (yellow) line represents the ATLAS (CMS) recent measurements on the $h\to\ \gamma\gamma$ channel, while the blue one is their combined result.*

the reasons for that is due to the fact that the electroweak phase transition (EWPT) is not strongly first order, which is required to suppress the sphaleron processes in the broken phase. The strength of the EWPT can be improved if there are new scalar degrees of freedom around the electroweak scale coupled to the SM Higgs, which is the case in the model that we are considering in this paper.

The investigation of the transition dynamics and its strength requires the precise knowledge of the effective potential of the CP-even scalar fields at finite temperature [27]. The zero temperature one-loop Higgs effective potential is given in the $\overline{DR}$ scheme by

$$V^{T=0}(h) = \frac{\lambda}{4!}h^4 - \frac{\mu^2}{2}h^2 + \sum_i n_i \frac{m_i^4(h)}{64\pi^2}\left(\ln\left(\frac{m_i^2(h)}{\Lambda^2}\right) - \frac{3}{2}\right), \tag{5.1}$$

where $h = (\sqrt{2}Re(H^0) - v)$ is the real part of the neutral component in the doublet, n_i are the field multiplicity, $m_i^2(h)$ is a field-dependent mass squared which are given in Appendix B, and Λ is the renormalization scale which we choose to be the top quark mass. At tree-level, the parameter μ^2 in the potential is given by $\mu^2 = \lambda v^2$, but if the one-loop corrections are considered, the parameter μ^2 is corrected by the counter-term

$$\delta\mu^2 = \sum_i \frac{n_i}{v}\frac{dm_i^2}{d\tilde{h}}\frac{m_i^2}{32\pi^2}\left(\ln\left(\frac{m_i^2}{\Lambda^2}\right) - 1\right)\Big|_{h=v,\mu^2\equiv\mu^2+\delta\mu^2}, \tag{5.2}$$

For instance, the one loop correction to the Higgs mass due to the charged singlets, when

neglecting the Higgs and gauge bosons contributions, is

$$m_h^2 \simeq 2\lambda v^2 + \sum_i \frac{\lambda_i^2 v^2}{16\pi^2} \ln \frac{m_{S_i}^2}{m_t^2}, \tag{5.3}$$

where the first term on the right hand side of the equation is the Higgs mass at the tree level. If one takes $m_{S_1} = m_{S_2} = 2m_t$ and $\lambda_1 = \lambda_2$, then the Higgs mass is exactly 125 GeV for $\lambda = 10^{-1}$, 10^{-2}, 10^{-3} if $\lambda_1 = 1.82$, 3.68, 3.82, respectively. Note that these values are still within the perturbative regime. On the other hand, these extra corrections could be negative and may relax the large tree-level mass value of the Higgs to its experimental value for λ large. Therefore, it is expected that these extra charged scalars will help the EWPT to be strongly first order by enhancing the value of the effective potential at the wrong vacuum at the critical temperature without suppressing the ratio $v(T_c)/T_c$, and therefore avoiding the severe bound on the mass of the SM Higgs.

In order to generate a baryon asymmetry at the electroweak scale [28], the anomalous violating $B + L$ interactions should be switched-off inside the nucleated bubbles, which implies the famous condition for a strong first order phase transition [29]

$$v(T_c)/T_c > 1, \tag{5.4}$$

where T_c is the critical temperature at which the effective potential exhibits two degenerate minima, one at zero and the other at $v(T_c)$. Both T_c and $v(T_c)$ are determined using the full effective potential at finite temperature [27]

$$V_{eff}(h,T) = V^{T=0}(h) + \tfrac{T^4}{2\pi^2} \sum_i n_i J_{B,F}\left(m_i^2/T^2\right) + V_{ring}(h,T); \tag{5.5}$$

with

$$J_{B,F}(\alpha) = \int_0^\infty x^2 \log(1 \mp \exp(-\sqrt{x^2+\alpha})), \tag{5.6}$$

and

$$V_{ring}(h,T) = -\frac{T}{12\pi} \sum_i n_i \left\{\tilde{m}_i^3(h,T) - m_i^3(h)\right\}, \tag{5.7}$$

where the summation is performed over the scalar longitudinal gauge degrees of freedom, and $\tilde{m}_i^2(h,T)$ are their thermal masses, which are given in Appendix B. The contribution (5.7) is obtained by the resummation of an infinite class of of infrared divergent multi-loops, known as the ring (or daisy) diagrams, which describes a dominant contribution of long distances and gives significant contribution when massless states appear in a system. It amounts

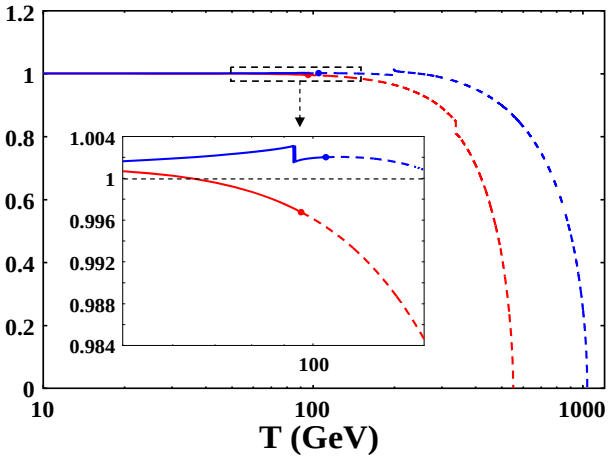

FIG. 7: *The dependance of the Higgs vev scaled by the zero temperature value* $\upsilon = 246$ *GeV , on the temperature below (solid lines) and above (dashed lines) the critical temperature for two benchmarks, where the red (blue) one corresponds to small (large)* λ *value and the positive (negative) scalar contributions in (5.3) relax the Higgs mass to it experimental value.*

to shifting the longitudinal gauge boson and the scalar masses obtained by considering only the first two terms in the effective potential [30]. This shift in the thermal masses of longitudinal gauge bosons and not their transverse parts tends to reduce the strength of the phase transition. The integrals (5.6) is often estimated in the high temperature approximation, however, in order to take into account the effect of all the (heavy and light) degrees of freedom, we evaluate them numerically.

In the SM, the ratio $\upsilon(T_c)/T_c$ is approximately $(2m_W^3 + m_Z^3) / (\pi \upsilon m_h^2)$, and therefore the criterion for a strongly first phase transition is not fulfilled for $m_h > 42$ GeV. However, if the one-loop corrections in (5.3) are sizeable, then this bound could be be relaxed in such a way that the Higgs mass is consistent with the measured value at the LHC. This might be possible since the extra charged singlets affect the dynamics of the SM scalar field VEV around the critical temperature [31].

This is shown in Fig. 7, where one sees the evolution of $\upsilon(T)$ with respect to the temperature. In contrast to the SM, where the EW vev decays quickly to zero just around $T \sim 100$ GeV, here it is delayed up to TeV due to the existence of the extra charged scalars. This can be understood due to the fact that the value of the effective potential at the wrong vacuum ($< h >= 0$) is temperature-dependant through the charged scalars thermal masses

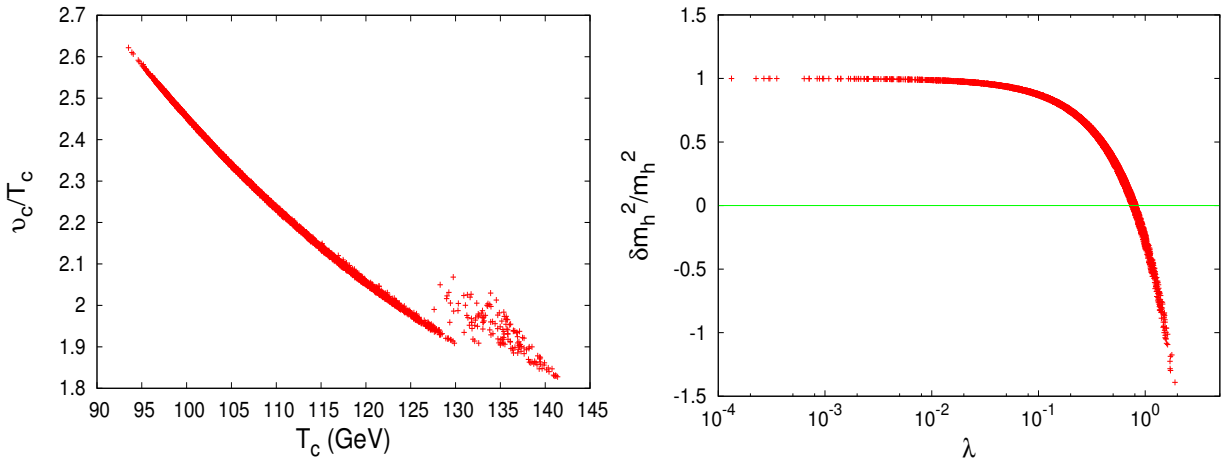

FIG. 8: *In the left figure, the critical temperature is presented versus the quantity υ_c/T_c in (5.4). In the right one, the relative contribution of the one-loop corrections (including the counter-terms) to the Higgs mass versus the parameter λ.*

in the symmetric phase. The evolution of the effective potential at this (wrong) minimum makes the transition happening at $T \geq 100$ GeV, while the Higgs vev is slowly decaying with respect to the temperature as shown in Fig.7.

In Fig. 8, we show two plots: one for $\upsilon(T_c)/T_c$ versus the critical temperature, and the second one for the dependence of the one loop correction to the Higgs mass on its quartic coupling for the same sets of parameters used in Fig. 6 in the previous section. It is worth noting that the parameters η_1, η_2 and η_{12} in (2.2) do not play a significant role in the dynamics of the EWPT, and therefore we fixed them in such a way to avoid the existence of electric charge breaking minima.

From the left panel in Fig. 8, we can see that one can have a strongly first order EWPT while the critical temperature lies around 100 GeV. The right panel shows that the one-loop contribution to the Higgs mass can be large compared to its tree-level value for small values of the self coupling λ. For larger values of λ, this contribution can be negative in order to bring the large tree-level Higgs mass down to its experimental value. Therefore, the EWPT can easily be strongly first order without being in conflict with the measured value of the Higgs mass.

Another issue in the investigation of the EWPT that could have impacts on collider signatures is the possible connection between the EWPT strength and the value of the mass-dimension triple Higgs coupling λ_3 as first discussed in [32]. In order to show this

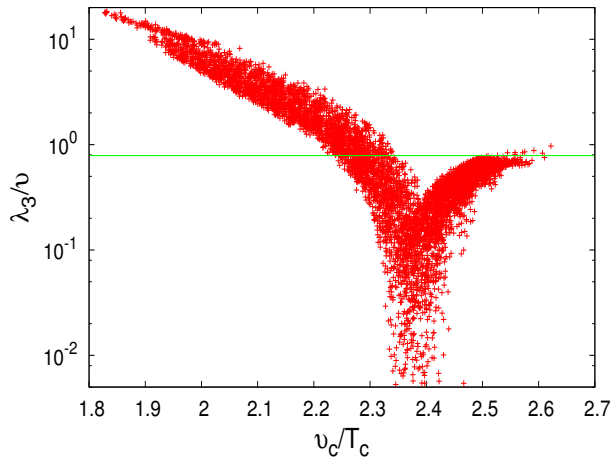

FIG. 9: *The triple Higgs coupling λ_3 in absolute value estimated at one loop in units of the Higgs vev; is shown versus the quantity υ_c/T_c in (5.4). The green line represents the tree-level value, and the corresponding benchmarks are the cases where different one-loop correction cancel each other.*

correlation between the EWPT strength and the enhancement on the triple Higgs coupling due to the non-decoupling loop effect of the additional charged singlets, we use the same values of the parameters of Fig. 8; and plot the triple Higgs coupling scaled the Higgs vev versus the EWPT strength, i.e., the ratio (5.4) as shown in Fig. 9.

It is clear that the triple Higgs coupling one-loop corrections could be very large with respect to the tree-level value for $v_c/T_c \lesssim 2.2$.

According to the ILC physics subgroup, the triple Higgs coupling can be measured with about 20% accuracy or better at $\sqrt{s} = 500$ GeV with integrated luminosity $\mathcal{L} = 500\ fb^{-1}$ [33]. This implies that for large parameter space, the model can be potentially testable at future linear colliders.

VI. COLLIDER PHENOMENOLOGY

Since the RH neutrinos couple to the charged leptons, one except them to be produced at e^-e^+ colliders, such as the ILC and CLIC with a collision energy $\sqrt{s}$ of few hundreds GeV up to TeV. If the produced pairs are the form $N_{2,3}N_{2,3}$ or $N_1N_{2,3}$, then $N_{2,3}$ will decay into charged lepton and $S_2^\pm$, and subsequently $S_2^\pm$ will decay into N_1 and a charged lepton.

If such decays occur inside the detector, then the signal will be

$$\begin{cases} \not{E} + 2\ell_R, \text{ for } \quad e^+e^- \to N_1 N_{2,3} \\ \not{E} + 4\ell_R, \text{ for } \; e^+e^- \to N_{2,3} N_{2,3}. \end{cases}$$

However, for $m_{N_i} \geq 100$ GeV, it is very possible that the decay $N_{2,3} \to N_1 + 2\ell_R$ occurs outside the detector, and thus escapes the detection. In this section, we assume that this is the case. Therefore, we analyze the production of all possible pairs of RH neutrinos, tagged with a photon from an initial state radiation, that is $e^-e^+ \to N_i N_k \gamma$ (with $i, k = 1, 2, 3$), where one searches for a high p_T gamma balancing the invisible RH neutrinos.

If the emitted photon is soft or collinear, then one can uses the soft/collinear factorization form [34]

$$\frac{d\sigma\left(e^+e^- \to N_i N_k \gamma\right)}{dx d\cos\theta} \simeq \mathcal{F}(x, \cos\theta)\hat{\sigma}\left(e^+e^- \to N_i N_k\right), \tag{6.1}$$

with $x = 2E_\gamma/\sqrt{s}$, here θ is the angle between the photon and electron and $\hat{\sigma}$ is the cross section (6.6) evaluated at the reduced center of mass energy $\hat{s} = (1-x)s$. The function $\mathcal{F}$ has a universal form

$$\mathcal{F}(x, \cos\theta) = \frac{\alpha_{em}}{\pi} \frac{1 + (1-x)^2}{x} \frac{1}{\sin^2\theta}. \tag{6.2}$$

Collinear photon with the incident electron or positron could be a good positive signal, especially if the enhancement in (6.1) is more significant than the SM background.

There are two leading SM background processes: a) the neutrino counting process $e^-e^+ \to \nu\bar{\nu}\gamma$ from the t-channel W exchange and the s-channel Z exchange, and b) the Bhabha scattering with an extra photon $e^-e^+ \to e^-e^+\gamma$, which can mimic the N_iN_i signature when the accompanying electrons or photons leave the detector through the beam pipe [35]. In addition to putting the cut on the energy of the emitted photon, one can reduce further the mono-photon neutrino background, by polarizing the incident electron and positron beams such that

$$\frac{N_{e_R^-} - N_{e_L^-}}{N_{e_R^-} + N_{e_L^-}} >> 50\%; \qquad \frac{N_{e_R^+} - N_{e_L^+}}{N_{e_R^+} + N_{e_L^+}} << 50\%, \tag{6.3}$$

where $N_{e^-_{L,R}}$ and $N_{e^+_{L,R}}$ are the number densities of the left (right)-handed electrons and positrons per unit time in the beam. At $\sqrt{s} >> 100$ GeV the process $e^-e^+ \to \nu\bar{\nu}\gamma$ is dominated by the W-exchange, and hence one expect that having the electron (positron) beam composed mostly of polarized right handed (left handed) electrons (positron) reduces this background substantially, whereas the signal increases since N_i couples to the right handed electrons.

Now, let us estimate the total cross section $\sigma\left(e^+e^- \to N_i N_k\right)$, which is basically the reverse of one of the processes which determines the effective dark matter density for coannihilation, at a collision energy of $\sqrt{s}$. The differential cross section of $e^+e^- \to N_i N_k$ for the energy $\sqrt{s}$ is given by [18]

$$\frac{d\sigma\left(e^+e^-\to N_i N_k\right)}{d\cos\theta} = \kappa_{ik}\frac{\left|g_{ie}g_{ke}^*\right|^2}{128\pi}\frac{\beta_{ik}}{s}\left(\frac{\left(\tilde{t}-x_i\right)\left(\tilde{t}-x_k\right)}{\left(\tilde{t}-x_s\right)^2}+\frac{(\tilde{u}-x_i)(\tilde{u}-x_k)}{(\tilde{u}-x_s)^2}-\frac{2\sqrt{x_i x_k}}{\left(\tilde{t}-x_s\right)(\tilde{u}-x_s)}\right), \tag{6.4}$$

with $\kappa_{ik} = 1/2$ if the two RH neutrinos are identical and equal to one if they are different, θ is the angle between the incoming electron and the outgoing N_i, and

$$\begin{aligned} x_j = m_{Nj}^2/s,\ x_s = m_{S_2}^2/s,\ \beta_{ik} = \sqrt{\left(1-x_i-x_k\right)^2-4x_i x_k} \\ \tilde{t} = \frac{t}{s} = \tfrac{x_i+x_k}{2} - \tfrac{1}{2}\left(1-\beta_{ik}\cos\theta\right),\ \tilde{u} = \frac{u}{s} = \tfrac{x_i+x_k}{2} - \tfrac{1}{2}\left(1+\beta_{ik}\cos\theta\right), \end{aligned} \tag{6.5}$$

By integrating over $\cos\theta$, the total cross section reads

$$\sigma\left(e^+e^- \to N_i N_k\right) = \kappa_{ik}\frac{\left|g_{ie}g_{ke}^*\right|^2}{32\pi}\frac{\beta_{ik}}{s}\left\{1+\frac{4\left[x_s^2-x_i x_s-x_k x_s+x_i x_k\right]}{w^2-\beta_{ik}^2}+\frac{w^2+w+2\sqrt{x_i x_k}}{\beta_{ik}w}\ln\left(\frac{w-\beta_{ik}}{w+\beta_{ik}}\right)\right\}, \tag{6.6}$$

with $w = -1 + x_i + x_k - 2x_s$. In order to estimate the differential cross section of the process $e^+e^- \to N_i N_k \gamma$ we integrate (6.1) over θ taking into account the minimum value of electromagnetic calorimeter acceptance in the ILC to be $\sin\theta > 0.1$ [36].

In Fig. 10, we show the photon spectrum for two values of collision energies $\sqrt{s} = 500$ GeV and 1 TeV. These plots are estimated using the factorization formula (6.1), however, we obtain similar results using CalcHEP [37]. We see that for the benchmark shown in Fig. 10, the heaviest RN is largely produced due to its large couplings to the electron/positron. Thus, for this particular benchmark the missing energy is dominated not by the DM, but rather by the other RH neutrinos.

VII. CONCLUSION

In this paper, we analyzed a radiative model for neutrino masses, generated at three loop level. Beside it can accommodate the neutrino oscillation data and be consistent with the LFV processes, it provides a DM candidate with a mass lying between few GeV up to 225 GeV; and a relatively light charged scalar, $S_2^\pm$, with a mass below 245 GeV. Furthermore, we showed that the charged scalar singlets can give an enhancement for $B\left(h \to \gamma\gamma\right)$, whereas

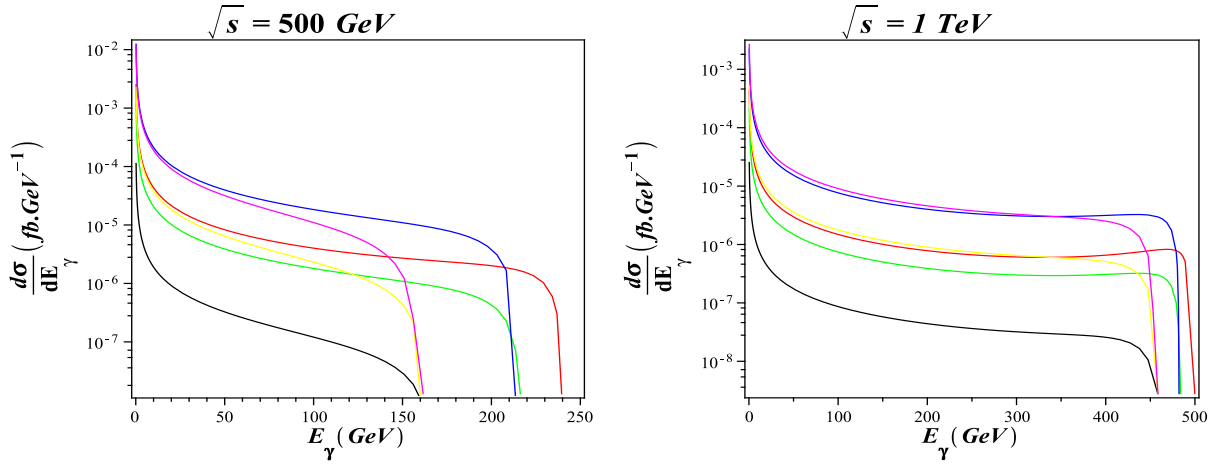

FIG. 10: *The photon spectra from the processes* $e^+e^- \to N_iN_k\gamma$ *where the curves: red, green, black, blue, yellow, magenta correspond to (i,k)=(1,1), (1,2), (2,2), (1,3), (2,3), (3,3) respectively. Here, we considered the following favored mass values:* $m_{N_1} = 52.53$ *GeV,* $m_{N_2} = 121.80$ *GeV,* $m_{N_3} = 126.19$ *GeV,* $m_{S_2} = 144.28$ *GeV, and the coupling values:* $g_{1e} = -4.19 \times 10^{-2}$, $g_{2e} = 2.10 \times 10^{-2}$ *and* $g_{3e} = -6.75 \times 10^{-2}$.

the decay $B\,(h \to \gamma Z)$ get a small suppression, compared to the SM. We also find that charged scalars with masses close the electroweak scale make the electroweak phase transition strongly first order. Since N_1 couples only to leptons, it can not be observed in experiments for direct dark matter searches. However it might be possible to search for such particle in indirect detection experiments, such as Fermi-LAT, and at future linear colliders, such as the international linear collider (ILC). Thus, for this particular benchmark the missing energy is dominated not by the DM, but rather by the other RH neutrinos.

Acknowledgments

We would like to thank S. Kanemura for his careful reading and useful comments on the manuscript. We also thank R. Soualah for the useful discussion on the search for DM at collider. This work is supported by the Algerian Ministry of Higher Education and Scientific Research under the PNR '*Particle Physics/Cosmology: the interface*', and the CNEPRU Project No. *D01720090023*.

Appendix A: Exact Neutrino Mass

According to Fig. 2.2, the neutrino mass matrix element $[\alpha,\beta]$ is given by

$$(M_\nu)_{\alpha\beta} = 2\int \frac{d^4Q_1}{(2\pi)^4}\int \frac{d^4Q_2}{(2\pi)^4}\frac{i}{Q_1^2-m_{S_1}^2}\left(-2if_{\alpha i}\right)P_L\frac{i}{\not{Q}_1-m_{\ell_i}}\times$$
$$i\Gamma_{ik}\left(Q_1,Q_2,-Q_1,-Q_2\right)\frac{i}{\not{Q}_2-m_{\ell_k}}P_L\left(-2if_{\beta k}\right)\frac{i}{Q_2^2-m_{S_1}^2}, \tag{A1}$$

with $P_{L,R}=(1\mp\gamma_5)/2$, and the effective vertex $\Gamma_{ik}(p_1,p_2,k_1,k_2)$ is a function of the momenta $p_{1,2}$ and $k_{1,2}$ for charged leptons and scalars, respectively, which is given by

$$i\Gamma_{ik}\left(p_1,p_2,k_1,k_2\right)=\int\frac{d^4k}{(2\pi)^4}\left(-ig_{ij}\right)P_L\frac{i\left(\not{k}+m_{N_j}\right)}{k^2-m_{N_j}^2}P_L\left(-ig_{kj}\right)\frac{i}{(k+p_1)^2-m_{S_2}^2}\left(-i\lambda_s\right)\frac{i}{(k-p_2)^2-m_{S_2}^2}. \tag{A2}$$

Then the neutrino mass matrix element $[\alpha,\beta]$ is

$$(M_\nu)_{\alpha\beta}=8f_{\alpha i}f_{\beta k}m_{\ell_i}m_{\ell_k}\lambda_s g_{ij}g_{kj}m_{N_j}P_L\int\frac{d^4k}{(2\pi)^4}\frac{1}{\left(k^2-m_{N_j}^2\right)}\times$$
$$\int\frac{d^4Q_1}{(2\pi)^4}\frac{1}{\left(Q_1^2-m_{\ell_i}^2\right)\left(Q_1^2-m_{S_1}^2\right)\left((k+Q_1)^2-m_{S_2}^2\right)}\int\frac{d^4Q_2}{(2\pi)^4}\frac{1}{\left(Q_2^2-m_{\ell_k}^2\right)\left(Q_2^2-m_{S_1}^2\right)\left((k+Q_2)^2-m_{S_2}^2\right)}, \tag{A3}$$

and since we have

$$\frac{1}{\left(Q^2-m_0^2\right)\left(Q^2-m_1^2\right)}=\frac{1}{m_1^2-m_0^2}\left(\frac{1}{Q^2-m_1^2}-\frac{1}{Q^2-m_0^2}\right), \tag{A4}$$

thus

$$\int\frac{d^4Q}{(2\pi)^4}\frac{1}{\left(Q^2-m_0^2\right)\left(Q^2-m_1^2\right)\left((k+Q)^2-m_2^2\right)}=\frac{i\left(B_0\left(k^2,m_1^2,m_2^2\right)-B_0\left(k^2,m_0^2,m_2^2\right)\right)}{16\pi^2m_1^2}, \tag{A5}$$

where the B_0 Passarino-Veltman function is [38]

$$B_0\left(k^2,m_1^2,m_2^2\right)=\frac{1}{\epsilon}-\int_0^1 dx\ln\frac{-x(1-x)k^2+(1-x)m_1^2+xm_2^2}{\mu^2}. \tag{A6}$$

Then, by neglecting the charged lepton masses, and making Wick rotation, we get

$$(M_\nu)_{\alpha\beta}=i\frac{\lambda_s m_{\ell_i}m_{\ell_k}}{(4\pi^2)^3m_{S_2}}f_{\alpha i}f_{\beta k}g_{ij}g_{kj}F\left(m_{N_j}^2/m_{S_2}^2,m_{S_1}^2/m_{S_2}^2\right), \tag{A7}$$

with

$$F\left(\alpha,\beta\right)=\frac{\sqrt{\alpha}}{8\beta^2}\int_0^\infty dr\frac{r}{r+\alpha}\left(\int_0^1 dx\ln\frac{x(1-x)r+(1-x)\beta+x}{x(1-x)r+x}\right)^2. \tag{A8}$$

Appendix B: Thermal Masses

The thermal masses are given as $\tilde{m}_i^2(h) = m_i^2(h) + \Pi_i(T)$, where $m_i^2(h)$ and $\Pi_i(T)$ are the field-dependant masses and the thermal self-energies respectively. In this model, the field-dependant masses are given by

$$\begin{aligned} &m_W^2 = g_2^2\tfrac{h^2}{4},\ m_t^2 = y_t^2\tfrac{h^2}{2},\ m_\chi^2 = -\mu^2 + \lambda\tfrac{h^2}{6},\ m_h^2 = -\mu^2 + \lambda\tfrac{h^2}{2}, \\ &m_{S_i}^2 = m_i^2 + \lambda_i\tfrac{h^2}{2},\ m_{W^3}^2(h) = g_2^2\tfrac{h^2}{4},\ m_{W^3-B}^2(h) = g_2 g_1\tfrac{h^2}{4},\ m_B^2(h) = g_1^2\tfrac{h^2}{4}, \end{aligned} \tag{B1}$$

where the diagonalization of the $\{W^3 - B\}$ matrix gives the massless photon and Z mass $m_Z^2 = (g_2^2 + g_1^2)\,h^2/4$. The thermal self-energies, that are generally estimated in the high temperature approximated as $\Pi_i \sim T^2$. In this model, these thermal self-energies are given by

$$\begin{aligned} \Pi_h = \Pi_\chi &= T^2\left\{\frac{\lambda}{12} + \frac{3g_2^2 + g_1^2}{16} + \frac{y_t^2}{4} + \frac{\lambda_1}{6} + \frac{\lambda_2}{6}\right\}, \\ \Pi_{W^\pm} = \Pi_{W^3} &= \frac{11}{6}g_2^2T^2,\ \Pi_{W^3-B} = 0, \\ \Pi_B &= \frac{11}{6}g_1^2T^2 + \frac{1}{6}g_1^2T^2 + \frac{1}{6}g_1^2T^2. \\ \Pi_{S_1} &= T^2\left\{\frac{\lambda_1}{3} + \frac{\eta_1}{6} + \frac{\eta_{12}}{6}\right\}, \\ \Pi_{S_2} &= T^2\left\{\frac{\lambda_2}{3} + \frac{\eta_{12}}{6} + \frac{\eta_2}{6}\right\}. \end{aligned} \tag{B2}$$

The last two terms in Π_h, Π_χ, Π_B, Π_{S_1} and Π_{S_2} represent the thermal loop contributions of $S_1^\pm$ and $S_2^\pm$ respectively.

---

[1] P. Minkowski, Phys. Lett. B 67, 421 (1977); M. Gell-Mann, P. Ramond and R. Slansky, Proceedings of the Supergravity Stony Brook Workshop, New York 1979, eds. P. Van Nieuwenhuizen and D. Freedman; T. Yanagida, Proceedings of the Workshop on Unified Theories and Baryon Number in the Universe, Tsukuba, Japan 1979, eds. A. Sawada and A. Sugamoto; R. N. Mohapatra and G. Senjanovic, Phys. Rev. Lett. 44, 912 (1980); J. Schechter and J. W. F. Valle, Phys. Rev. D 22, 2227 (1980).

[2] M. Fukugita and T. Yanagida, Phys. Lett. B 174, 45 (1986).

[3] F. Vissani, Phys. Rev. D 57, 7027 (1998); J. Elias-Miro, J.R. Espinosa, G.F. Giudice, H.M. Lee and A. Strumia, JHEP 1206, 031 (2012).

[4] A. Zee, Phys. Lett. B 161, 141 (1985).

[5] X.-G. He, Eur. Phys. J. C 34, 371-376 (2004); P.H. Frampton, M.C. Oh and T. Yoshikawa, Phys. Rev. D 65, 073014 (2002).

[6] K.S. Babu, Phys. Lett. B 203, 132 (1988).

[7] L.M. Krauss, S. Nasri and M. Trodden, Phys. Rev. D 67, 085002 (2003).

[8] M. Aoki, S. Kanemura and O. Seto, Phys. Rev. Lett. 102, 051805 (2009); Phys. Rev. D 80, 033007 (2009); M. Aoki, S. Kanemura, K. Yagyu, Phys. Rev. D 83, 075016 (2011).

[9] M. Gustafsson, J.M. No and M.A. Rivera, arXiv:1212.4806 [hep-ph].

[10] K. Cheung and O. Seto, Phys. Rev. D 69, 113009 (2004).

[11] J. Adam et al. [MEG Collaboration], arXiv:1303.0754 [hep-ex].

[12] J. Beringer et al. (Particle Data Group), Phys. Rev. D 86, 010001 (2012).

[13] G. Aad et al. (ATLAS Collaboration), Phys. Lett. B 716, 1-29 (2012).

[14] S. Chatrchyan et al. (CMS Collaboration), Phys. Lett. B 716, 30-61 (2012).

[15] B. Pontecorvo, Sov. Phys. JETP 26, 984 (1968); Z. Maki, M. Nakagawa and S. Sakata, Prog. Theor. Phys. 28, 870 (1962).

[16] D.V. Forero, M. Tortola and J.W.F. Valle, Phys. Rev. D 86, 073012 (2012).

[17] E. Ma and M. Raidal, Phys. Rev. Lett. 87, 011802 (2001); Erratum-ibid. 87, 159901 (2001).

[18] K. Cheung and O. Seto, Phys. Rev. D 69, 113009 (2004).

[19] F. Simkovic, A. Faessler, H. Muther, V. Rodin and M. Stauf, Phys. Rev. C 79, 055501 (2009).

[20] F.T. Avignone, Nucl. Phys. Proc. Suppl. 143, 233 (2005); W. Rodejohann, J. Phys. G 39, 124008 (2012).

[21] P.A.R. Ade et al. [Planck Collaboration], arXiv:1303.5062 [astro-ph.CO].

[22] K. Kong and K.T. Matchev, JHEP 01, 038 (2006).

[23] L. Bergstrom, Phys. Rev. D 86, 103514 (2012).

[24] ATLAS Collaboration, Report No. ATLAS-CONF-2013-014, March 2013.

[25] C. Ochando [CMS Collaboration], Talk presented at Rencontres de Moriond, La Thuile, Italy, 9-16, March 2013.

[26] A. Djouadi, Phys. Rept. 457, 1 (2008).

[27] L. Dolan and R. Jackiw, Phys. Rev. D 9, 3320-3341 (1974); S. Weinberg, Phys. Rev. D 9, 3357-3378 (1974).

[28] V. Kuzmin, V. Rubakov and M.E. Shaposhnikov, Phys. Lett. B 155, 36 (1985).

[29] M.E. Shaposhnikov, Nucl. Phys. B 287, 757-775 (1987); ibid 299, 797-817 (1988).

[30] M.E. Carrington, Phys. Rev. D 45, 2933 (1992).

[31] A. Ahriche, Phys. Rev. D 75, 083522 (2007); A. Ahriche and S. Nasri, Phys. Rev. D 83, 045032 (2011); Phys. Rev. D 85, 093007 (2012).

[32] S. Kanemura, Y. Okada and E. Senaha, Phys. Lett. B 606, 361 (2005).

[33] H. Baer, et al., '*Physics at the International Linear Collider*', available at: http://lcsim.org/papers/DBDPhysics.pdf

[34] A. Birkedal, K. Matchev and M. Perelstein, Phys. Rev. D 70, 077701 (2004).

[35] C. Bartels, M. Berggren and J. List, Eur. Phys. J. C 72, 2213 (2012).

[36] J.A. Aguilar-Saavedra et al. [ECFA/DESY LC Physics Working Group Collaboration], hep-ph/0106315.

[37] A. Belyaev, N.D. Christensen and A. Pukhov, arXiv:1207.6082 [hep-ph].

[38] G. Passarino and M.J.G. Veltman, Nucl. Phys. B160, 151 (1979).